scientific reports

Check for updates

OPEN

BRD4 and MYB inhibition overcomes venetoclax resistance in *EVI1*-rearranged acute myeloid leukemia

Weijia Zang[1,2,3,11], Yui Koike[1,3,11], Koutarou Nishimura[1,3]✉, Atsushi Tanaka[3,4], Hiromi Yamazaki[1,3], Takaya Yamasaki[1], Hiromi Ito[1,3], Yifan Zhang[1,2,3], Yumi Aoyama[1,2,3], Wataru Saika[1,3,6], Muran Xiao[3], Chihiro Hasegawa[1,3,7], Hiroyoshi Kunimoto[8], Hideaki Nakajima[8], Fumihiko Ishikawa[9,10], Akifumi Takaori-Kondo[2] & Daichi Inoue[1,2,3,5]✉

***EVI1*-rearranged acute myeloid leukemia (AML) with inv(3)(q21q26) or t(3;3)(q21q26) represents a distinct and aggressive subtype characterized by poor prognosis and limited treatment options. However, the optimal strategy to overcome resistance to conventional therapy remains elusive. Building upon observations correlating *EVI1* overexpression with reduced sensitivity to venetoclax, a BH3-mimetic BCL-2 inhibitor, we investigated the mechanisms of resistance to venetoclax in combination with hypomethylating agents in inv(3)/t(3;3) AML cells. Utilizing novel murine models recapitulating inv(3) AML with concomitant *SF3B1* mutations, we conducted comprehensive phenotypic and transcriptomic analyses in the presence or absence of venetoclax-containing therapy. Despite initial therapeutic responses, manifested as partially prolonged survival and myeloid differentiation, resistant leukemic cells demonstrated enhanced dependency on BRD4 and MYB pathways with a dormant phenotype. Notably, inhibition of either BRD4 or MYB significantly augmented the efficacy of venetoclax and hypomethylating agents in both murine and patient-derived AML models harboring inv(3) and *SF3B1* mutations. These findings elucidate the transcriptional dynamics underlying venetoclax resistance and propose alternative therapeutic strategies targeting BRD4 and MYB as promising avenues for improving outcomes in patients with *EVI1*-rearranged AML. Our work highlights the necessity for innovative combination therapies to address the multifaceted mechanisms of resistance in this high-risk leukemia subtype.**

Keywords Acute myeloid leukemia, EVI1, Venetoclax, Hypomethylating agent, MYB, BRD4

Acute myeloid leukemia (AML) with inv(3)(q21q26) or t(3;3)(q21q26), classified as a distinct subtype by the World Health Organization classification, presents a formidable challenge in hematologic oncology[1]. This aggressive malignancy, referred to as "inv(3)/t(3;3) AML," is characterized by a dismal median overall survival of less than one-year post-diagnosis[2–5]. Similar genomic alterations observed in myelodysplastic syndromes (MDS) correlate with equally poor outcomes, underscoring the urgent need for improved therapeutic strategies[4,6]. Recent investigations have unveiled the molecular intricacies driving inv(3)/t(3;3) AML pathogenesis. The hallmark chromosomal rearrangements relocate the *GATA2* distal enhancer from its

[1]Department of Cancer Pathology, Graduate School of Medicine and Frontier Biosciences, The University of Osaka, Suita 565-0871, Japan. [2]Department of Hematology, Graduate School of Medicine, Kyoto University, Kyoto, Japan. [3]Department of Hematology-Oncology, Institute of Biomedical Research and Innovation, Foundation for Biomedical Research and Innovation at Kobe, Kobe, Japan. [4]Department of Hematology, Kyoto-Katsura Hospital, Kyoto, Japan. [5]Institute for Open and Transdisciplinary Research Initiatives, The University of Osaka, Suita, Japan. [6]Department of Hematology, Shiga University of Medical Science, Otsu, Japan. [7]Department of Hematology and Oncology, Graduate School of Medicine, The University of Osaka, Suita, Japan. [8]Department of Stem Cell and Immune Regulation, Graduate School of Medicine, Yokohama City University, Yokohama, Kanagawa, Japan. [9]Department of Comprehensive Pathology, Graduate School of Medical and Dental Sciences, Institute of Science Tokyo, Tokyo, Japan. [10]RIKEN Center for Integrative Medical Sciences, Yokohama, Japan. [11]Weijia Zang and Yui Koike have contributed equally to this work. ✉email: nishimura.koutarou.pww@osaka-u.ac.jp; inoue@patho.med.osaka-u.ac.jp

typical position at 3q21, transforming it into a potent super-enhancer that aberrantly activates the *EVI1* proto-oncogene, a critical driver of leukemogenesis within the *MDS1 And EVI1 Complex Locus* (*MECOM*) at 3q26. The enhancer contains multiple transcription factor (TF) binding sites, including those for MYB, RUNX1, and other key regulators of hematopoiesis[7,8]. *EVI1* originally encodes a TF crucial for normal hematopoiesis, characterized by two Zinc finger (ZF) DNA binding domains located at the N-terminus and the C-terminus of the protein, encompassing seven and three Zinc fingers, respectively[9]. A series of studies have demonstrated that *EVI1* overexpression promotes a stem-like gene expression program and dysregulates apoptotic pathways in hematopoietic progenitors, enhancing self-renewal capacity and contributing to chemotherapy resistance[10]. Furthermore, our recent findings have elucidated the mechanistic link between mutations in the splicing factor SF3B1 and RAS-related pathways, frequently co-occurring in inv(3)/t(3;3) leukemias[10]. Notably, we identified a novel oncogenic *EVI1* splicing variant caused by *SF3B1* mutation, highlighting the role of pathological splicing in disease progression[11].

The advent of venetoclax, a BH3-mimetic targeting BCL-2, in combination with hypomethylating agents, has shown promise in AML treatment, particularly for patients ineligible for intensive chemotherapy[12]. This combination leverages complementary mechanisms to promote apoptosis and inhibit leukemic cell survival. BH3 mimetics represent a promising class of anticancer drugs, exerting their effects by inhibiting pro-survival BCL-2 proteins, leading to apoptosis induction[13]. The BCL-2 protein family plays a critical role in regulating the intrinsic apoptosis pathway, comprising both pro-apoptotic and anti-apoptotic members. By binding to BCL-2, venetoclax displaces pro-apoptotic proteins like BIM, which then activate BAX and BAK, leading to mitochondrial outer membrane permeabilization with the cytochrome C release and subsequent cell death[14]. Maintaining the appropriate balance between these proteins is crucial for physiological hematopoiesis, with dysregulation commonly observed in hematological malignancies. Despite various studies demonstrating the efficacy of venetoclax in AML[15,16], the efficacy of this venetoclax regimen in *EVI1*-rearranged AML remains unclear, primarily due to the rarity of genetically accurate animal models and limited clinical analyses.

In this study, we delineate the response of inv(3)/t(3;3) AML cells to venetoclax and hypomethylating agent combination therapy, focusing on post-treatment transcriptional dynamics. Utilizing novel murine models that faithfully recapitulate the humanized inv(3)(q21q26) allele and *SF3B1* mutations[11], we observe a phenotypic shift in AML cells following an initial response and subsequent resistance to the combination therapy. Notably, these resistant cells exhibit heightened dependency on BRD4 and MYB pathways, suggesting potential avenues for second-line therapeutic interventions. Our findings not only elucidate the mechanistic underpinnings of venetoclax resistance in *EVI1*-rearranged AML but also propose alternative therapeutic strategies with promising clinical implications. This work addresses a critical gap in our understanding of this aggressive AML subtype and paves the way for more effective treatment approaches.

Results

EVI1-rearranged AML is relatively resistant to venetoclax

Inv(3)/t(3;3) acute myeloid leukemia (AML) is characterized by a dismal prognosis, with multiple studies reporting a median overall survival of less than one year post-diagnosis, whereas long-term overall survival is less than 15%[1–5,11]. Given the widespread efficacy of venetoclax in various AML subtypes, we sought to evaluate its sensitivity in inv(3)/t(3;3) AML. In vitro cytotoxicity assays, quantifying AML cell elimination after 72-hour exposure, demonstrated that inv(3)/t(3;3) AML cells exhibited markedly reduced sensitivity to venetoclax compared to *EVI1* wild-type AML (Fig. 1A). Chromosomal abnormalities involving 3q21 activate *EVI1* transcription via an ectopic *GATA2* enhancer. Notably, aberrant *EVI1* expression can occur without 3q26 rearrangements, observed in ~ 8–10% of myelodysplastic syndrome (MDS), 8% of de novo AML, and 30% of advanced chronic myeloid leukemia (CML)[17]. To further elucidate the relationship between *EVI1* expression and venetoclax sensitivity, we stratified AML samples into quartiles based on *EVI1* expression levels. Comparative analysis revealed that the *EVI1*-high group (highest quartile) exhibited significantly greater resistance to venetoclax compared to the *EVI1*-low group (lowest quartile) (Fig. 1B), suggesting a crucial role for the EVI1 TF in determining drug vulnerability. To gain deeper insights into the genomic landscape of inv(3)/t(3;3) myeloid neoplasms, we compiled data from prior cohorts (n = 622 from BeatAML, n = 200 from TCGA AML) with recently reported cohorts of 109 inv(3)/t(3;3) patients[18–20]. This comprehensive analysis revealed that the most frequently mutated genes in inv(3)/t(3;3) myeloid neoplasms included the core RNA splicing factor *SF3B1*, followed by RAS pathway genes (*NRAS*, *PTPN11*, *KRAS*, and *NF1*) and *GATA2* mutations (Fig. 1C). Statistical analysis using Fisher's exact test demonstrated that the mutational frequencies of these genes were significantly elevated in *EVI1*-rearranged patients compared with non-*EVI1*-rearranged patients. Strikingly, while *SF3B1* mutations are rare in the general AML population (~ 4%), inv(3)/t(3;3) AML was characterized by a significantly higher mutation rate (~ 30%) in this gene. Leveraging the integrated analysis of drug response in the BeatAML2.0 cohort[21], we demonstrated that *SF3B1* mutations are most strongly associated with increased resistance to venetoclax (Fig. 1D). Collectively, these findings underscore the distinct molecular and pharmacological profile of inv(3)/t(3;3) AMLs, particularly in terms of venetoclax response, and highlight the need for alternative therapeutic strategies for this high-risk AML subtype.

In vivo efficacy of venetoclax in inv(3) leukemia model

In our prior study, we generated *Mx1*-Cre: inv(3) *Sf3b1*$^{K700E/WT}$ mice by crossing transgenic mice harboring a human BAC (bacterial artificial chromosome) encompassing the human inv(3)(q21q26) allele[7] with mice carrying a conditional knock-in of mutant *Sf3b1*^{K700E}[22]. As we reported, the *Mx1*-Cre: inv(3) *Sf3b1*$^{K700E/WT}$ spontaneously developed aggressive leukemia[11]. We established a serial transplant model by injecting CD45.2$^+$ leukemic cells from these mice into the tail veins of lethally irradiated CD45.1$^+$ wild-type recipients. Recipients were divided into Vehicle control and venetoclax/decitabine (VEN/DAC) treatment (Fig. 2A), followed by

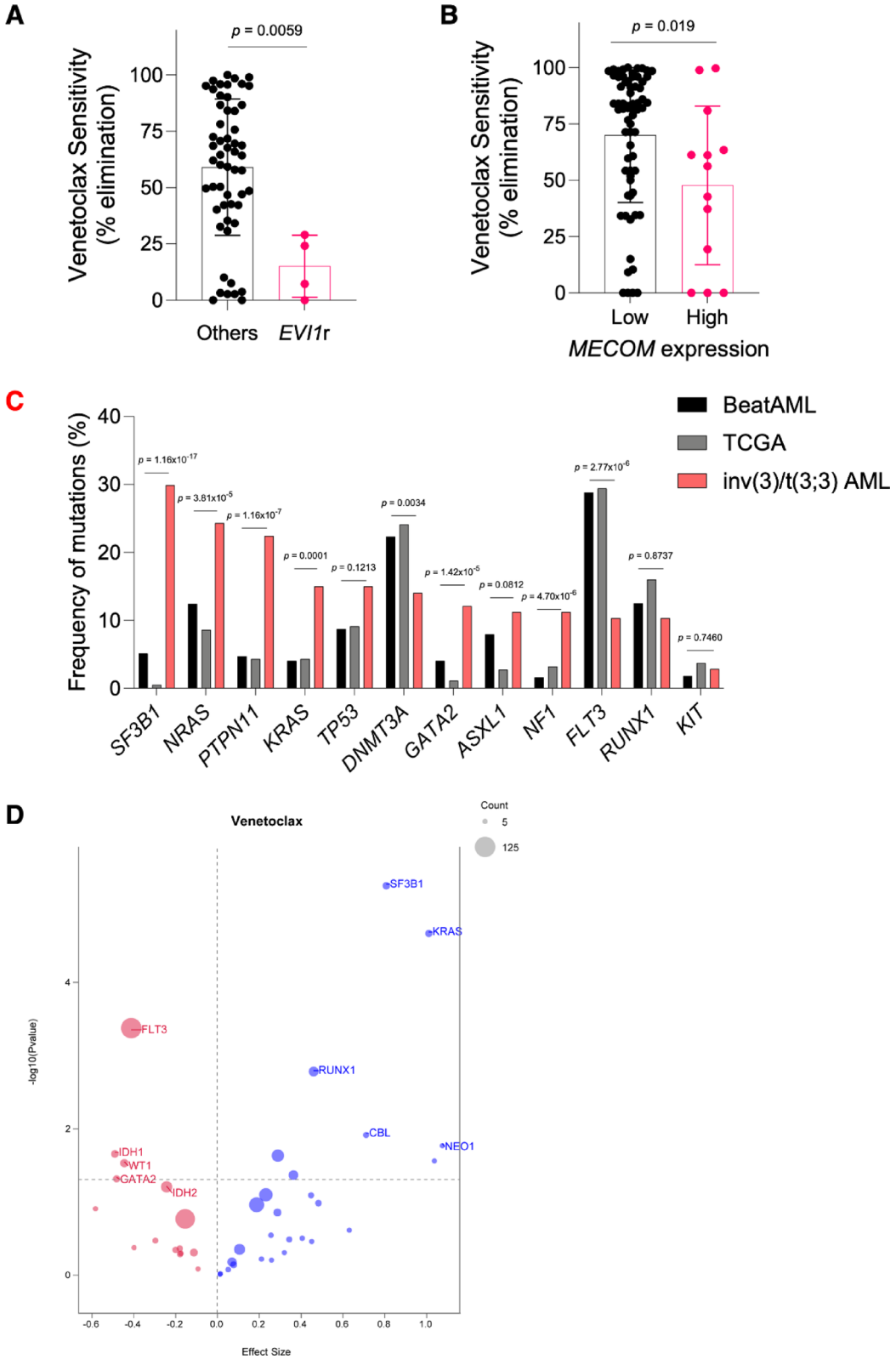

Fig. 1. Characterization of sensitivity to venetoclax in *EVI1*-rearranged AML cells. (**A**) Plot of venetoclax sensitivity quantified by the percentage of elimination of AML cells. Others $n = 55$, *EVI1*r $n = 4$. The *p*-value was calculated by a two-sided t-test. (**B**) Plot showing venetoclax sensitivity based on *MECOM* mRNA expression levels. Low (Normalized *MECOM* levels < 20), $n = 67$, and High (Normalized *MECOM* levels > 80), $n = 13$; the *p*-value was calculated using a two-sided t-test. (**C**) Bar chart displaying the mutational frequencies of the indicated genes across different patient cohorts: inv(3)/t(3;3) patients, $n = 109$; BeatAML, $n = 622$; TCGA AML, $n = 200$. *p*-values were calculated using Fisher's exact test. (**D**) Dot mapping of venetoclax resistance to the effects of mutated genes, data sourced from BeatAML2.0 cohort. The y-axis represents -log10 of *p*-values.

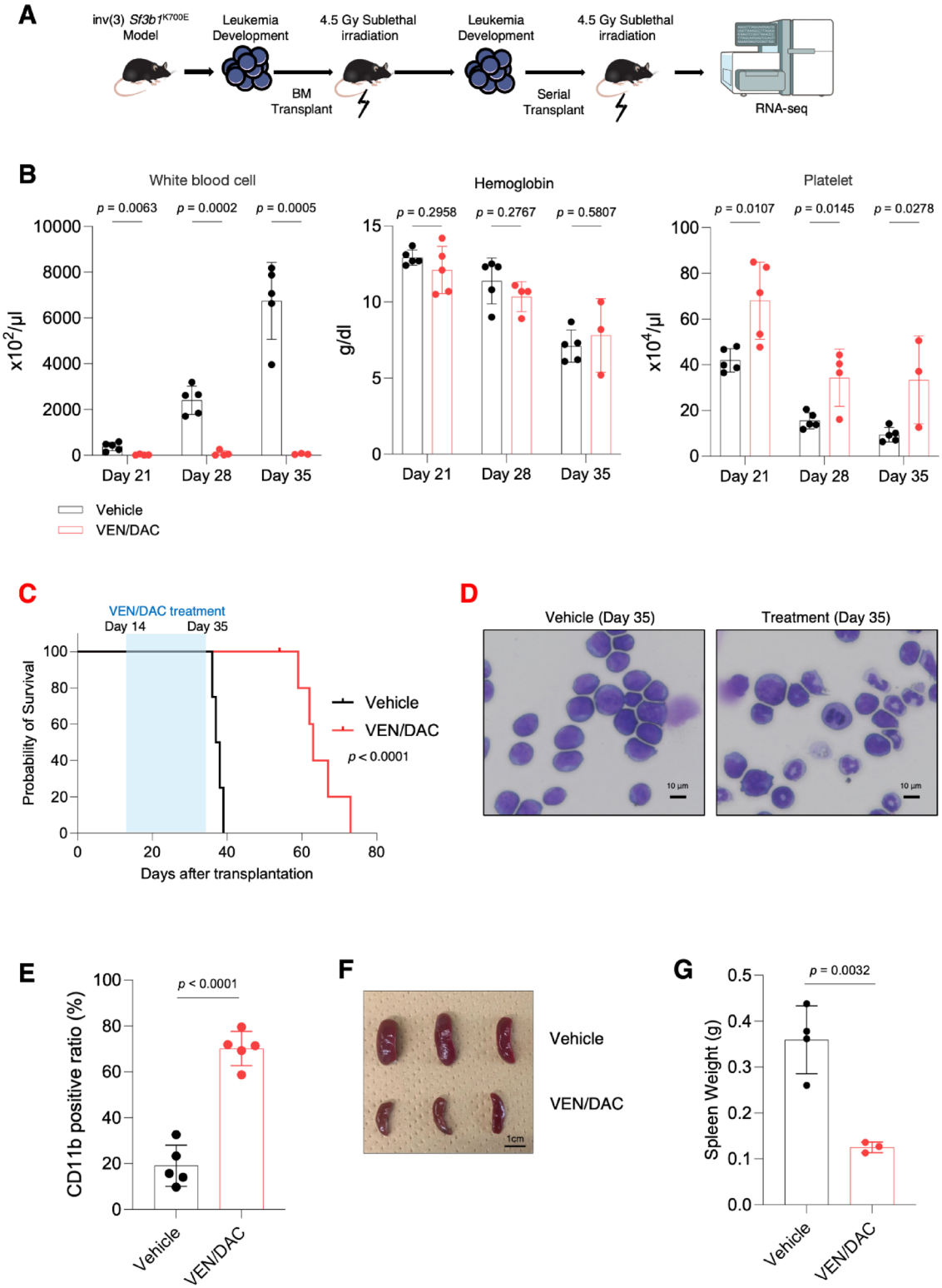

blood counts and survival monitoring. VEN/DAC treatment demonstrated a significant impact on leukemia progression, characterized by lower white blood cell counts and higher platelet counts (Fig. 2B). Combination treatment significantly prolonged recipient survival ($p < 0.0001$), although all mice eventually succumbed to leukemia around day 60 after transplant (Fig. 2C). Cytological examination of bone marrow (BM) samples revealed that VEN/DAC-treated mice exhibited more mature myeloid cell morphology and fewer blastic cells in cytospin-stained sections (Fig. 2D, Supplementary Fig. 1D). While the CD45.2$^+$ cell frequency in BM, spleen, and peripheral blood (PB) was nearly 100%, indicating the donor-derived leukemia, it decreased in the spleen and PB at day 35 (Supplementary Fig. 1E). Furthermore, flow cytometric analysis of donor-derived PB cells showed increased CD11b positivity in the treatment group, indicating enhanced maturation of inv(3) leukemic cells in response to VEN/DAC (Fig. 2E, Supplementary Fig. 1A). At the time of sacrifice, we observed reduced spleen

◀**Fig. 2**. Efficacy of VEN/DAC combination therapy in the inv(3) AML model. (**A**) Schema of inv(3) *Sf3b1*^{K700E} model bone marrow (BM) serial transplantation assays. (**B**) Plots of white blood cells, hemoglobin, and platelets in peripheral blood (PB) of recipient mice. $N = 5$ independent samples at transplant Day 0; data represent mean ± s.e.m. Statistical significance was calculated with a two-tailed unpaired t-test. (**C**) Kaplan-Meier survival curve of Vehicle ($n = 4$) and VEN/DAC treatment group ($n = 5$). Treatment of venetoclax (100 mg/kg, once a day, by oral gavage) and decitabine (0.25 mg/kg, every 48 h via intraperitoneal injection) was administered for three weeks (until Day 35), from Day 14 after transplantation. The *p*-value was calculated by the log-rank test. (**D**) Representative images of the BM cytospin, stained with Wright-Giemsa staining. Scale bar: 10 μm. (**E**) The proportion of CD11b in peripheral blood, $n = 5$ independent samples; data represent mean ± s.e.m. The *p*-value was calculated by a two-sided t-test. (**F**) Representative images of the spleen of Vehicle and VEN/DAC treatment mice. (**G**) Plot of spleen weight ($n = 4$, Vehicle group; $n = 3$, VEN/DAC treatment group). Data represent mean ± s.e.m. The *p*-value was calculated by a two-sided t-test.

size and weight in the treatment group (Fig. 2F, G), along with a significant decrease in absolute BM cell counts (Supplementary Fig. 1B). These findings demonstrate the in vivo efficacy of the VEN/DAC combination in an inv(3) leukemia model, although it exerts the short-term efficacy. While our results highlight the potential of this therapeutic approach in temporarily mitigating disease progression and improving hematological parameters, they also underscore the persistent challenge of achieving long-term remission in this aggressive AML subtype.

VEN/DAC treatment altered the phenotype of inv(3) leukemia cells

To elucidate the molecular mechanisms underlying the therapeutic effects of VEN/DAC combination treatment on inv(3)/t(3;3) AML, we performed comprehensive RNA-seq analysis on c-Kit$^+$ cells isolated via MACS sorting from both vehicle and VEN/DAC treatment groups. The principal component analysis (PCA) results exhibited significant differences between vehicle and VEN/DAC (Supplementary Fig. 2A). The Transcriptomic profiling revealed substantial differences in gene expression patterns between the two groups, with 392 genes significantly downregulated and 372 genes upregulated (adjusted *p*-value < 0.05 and |log2FC| > 2) (Fig. 3A, B and Supplementary Table 1). Notably, genes associated with mature myeloid markers, including *Lyz2*, *Cebpe*, *Fcnb*, and *Sirpa*, exhibited significant upregulation in the treatment group[23–26]. Conversely, stem cell-related genes such as *Zbtb16*, *Irs2*, and *Med12l* were markedly downregulated, suggesting a shift towards a more differentiated phenotype[27,28]. Further Gene Ontology (GO) and pathway enrichment analysis provided valuable insights into the biological processes modulated by VEN/DAC treatment. The Gene Ontology Biological Process analysis revealed significant upregulation of pathways associated with myeloid differentiation, including neutrophil degranulation, neutrophil activation, and neutrophil-mediated immunity (Fig. 3C). This finding aligns with the observed increase in CD11b positivity in our in vivo therapeutic model. Additionally, genes upregulated in the treatment group showed enrichment in pathways related to hemostasis and cell cycle (Fig. 3D), further corroborating the phenotypic changes observed in vivo. The enrichment of these specific pathways suggests a dual mechanism of action for VEN/DAC, involving both direct cytotoxicity and the induction of differentiation.

Differential gene expression in treated and resistant group

Our in vivo therapeutic experiments (Fig. 2A) demonstrated that while the VEN/DAC combination treatment effectively prolonged survival, all mice eventually succumbed to leukemia, with efficacy diminishing significantly after day 60 (Fig. 2C). This pattern aligns with our previous analysis of venetoclax resistance in AML patients with higher *MECOM* expression (Fig. 1B), suggesting the development of treatment resistance. By day 53, the morphology had reverted to a blastic phenotype (Supplementary Fig. 1C–E), and the CD45.2$^+$ donor-derived chimerism had returned to the levels observed in the untreated sample at day 35 (Supplementary Fig. 1E). To further elucidate the molecular basis of resistance, we conducted an additional RNA-seq analysis on c-Kit$^+$ cells MACS-sorted from treatment-responsive (Treatment group) and VEN/DAC-resistant mice (Resistant group) (Figs. 2C and 4A). Hierarchical clustering correlation analysis revealed distinct transcriptional profiles between these groups (Fig. 4B), indicating significant alterations in gene expression patterns during the development of resistance. Gene expression heatmap and pathway analysis of differentially expressed genes (DEGs) between treatment-responsive and resistant groups showed upregulation of cell cycle-related genes during the response phase of VEN/DAC treatment. However, this elevated expression was not maintained in the resistant phase (Fig. 4C, D, Supplementary Fig. 3A). This temporal shift in cell cycle-related gene expression patterns suggests an initial proliferative and cell cycle checkpoint response to treatment, followed by a more tolerant and quiescent state in resistant cells, potentially facilitating treatment evasion[29]. Further RNA-seq analysis revealed that the positive enrichment of TF substrates, including MYB, BRD4, and MECOM, represented a pathogenetic hallmark event that persisted from the VEN/DAC treatment phase through the resistant phase (Fig. 4E, F). These comprehensive molecular analyses provide crucial insights into the dynamic transcriptional landscape of inv(3) leukemia cells during treatment response and resistance development. The observed shifts in cell cycle-related pathways and TF activities highlight potential targets for overcoming resistance and improving the long-term efficacy of VEN/DAC combination therapy in this aggressive AML subtype.

Treatment efficacy with BRD4/MYB inhibitors in inv(3) AML cells

Our RNA-seq analysis unveiled the activation of unfavorable TF programs, notably BRD4 and MYB, providing comprehensive insights into the mechanisms underlying VEN/DAC resistance and highlighting potential therapeutic vulnerabilities (Fig. 4E). To assess the efficacy of BRD4 and MYB inhibitors in the context of VEN/DAC treatment, we employed these inhibitors in VEN/DAC-treated inv(3)/t(3;3) leukemic cells. The BRD4

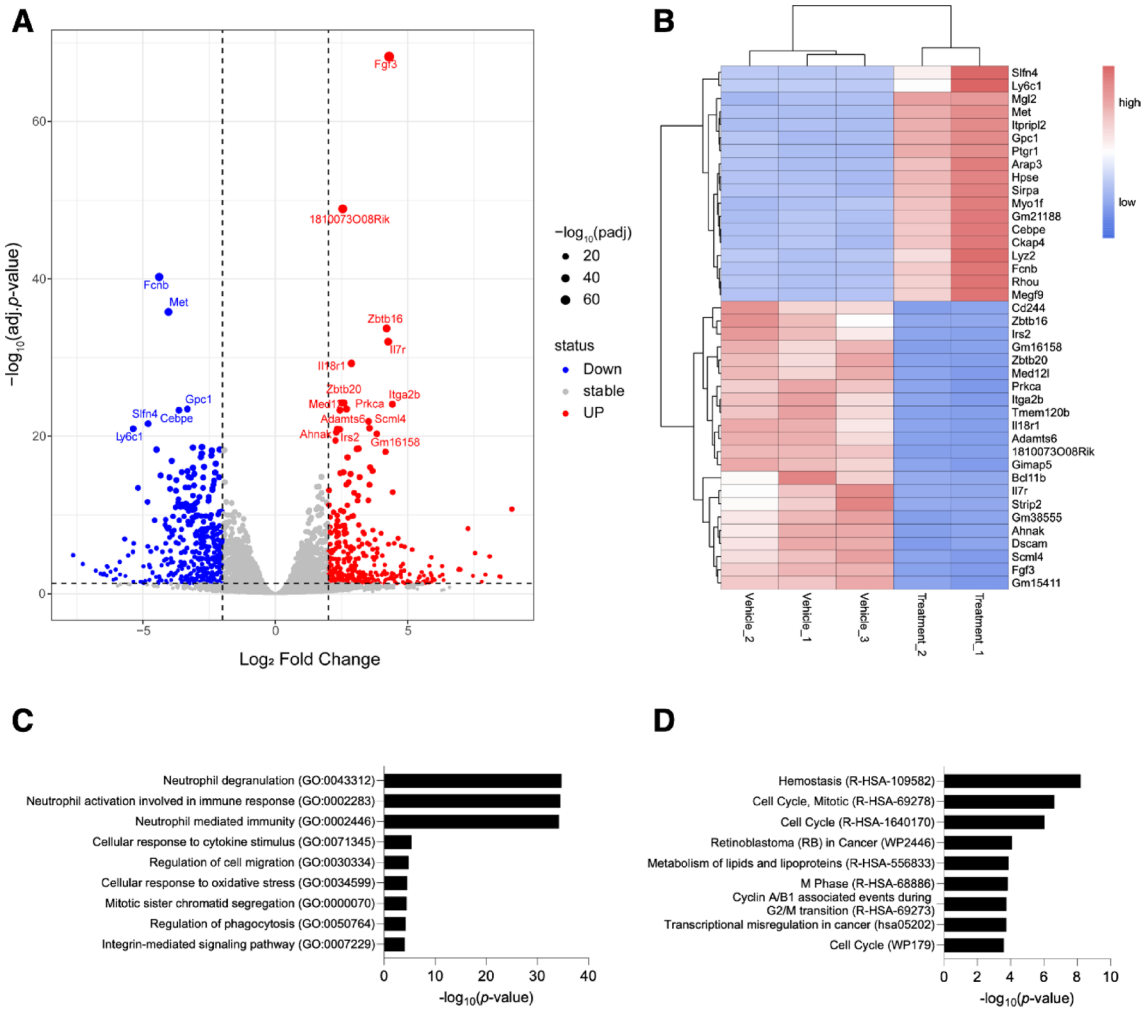

Fig. 3. Transcriptomic analysis of VEN/DAC-treated inv(3) AML model. (**A**) Volcano plot of differential mRNA expression between the VEN/DAC treatment group and Vehicle group. Upregulated genes in VEN/DAC treatment are highlighted in red, while downregulated ones are shown in blue, applying adjusted *p*-value < 0.05 and |log2FC| > 2. The x-axis represents log2 fold change (FC) values; the y-axis represents -log10 of adjusted *p*-values. (**B**) Heatmap showing the top 40 up- or down-regulated genes evaluated by RNA-seq (ranked by adjusted *p*-value) in the VEN/DAC treatment group. (**C**) Gene Ontology Biological Process (2018 version) enrichment of genes up-regulated in VEN/DAC treatment group. The *p*-values were calculated via Enrichr, the x-axis represents -log10 of *p*-values. (**D**) Reactome Pathway Analysis enrichment of genes up-regulated in VEN/DAC treatment group, the *p*-values were calculated via Enrichr, the x-axis represents -log10 of *p*-values.

inhibitors (JQ1[30] or ABBV-744[31]) demonstrated significant anti-leukemic effects, reducing myeloid colony formation in vitro and suppressing leukemic cell expansion in vivo through synergistic effects with VEN/DAC (Fig. 5A, B, Supplementary Fig. 4A). To further investigate the role of BRD4 inhibitors, we transplanted inv(3)/t(3;3) leukemic cells into sublethally irradiated wild-type recipients and administrated a combination treatment of VEN/DAC and JQ1. The addition of the BRD4 inhibitor JQ1 significantly reduced the proportion of inv(3) AML c-Kit$^+$ cells 6–7 weeks post-transplantation (Fig. 5C). Similarly, MYB inhibitors celastrol[32] and monensin[33] exhibited anti-leukemic properties. In vitro M3434 colony formation assays demonstrated that the MYB inhibitors, when combined with VEN/DAC at equivalent concentrations, synergistically inhibited inv(3) *Sf3b1*^{K700E} primary mouse cells and targeted the VEN/DAC resistance clones. (Fig. 5D-G).

Synergistic effects in human patient-derived inv(3) leukemic cells

We next investigated the synergistic effects of BRD4/MYB inhibitors in combination with VEN/DAC using human *EVI1*-rearranged AML cells to evaluate their potential clinical applicability. We utilized YCU-AML1 cell lines[34], recently established from a high-risk MDS/AML patient harboring inv(3) and *SF3B1* mutation. To investigate the BRD4 and MYB inhibition in YCU-AML1 cells, we evaluated the effect of combination treatments in vitro. MYB inhibitors, celastrol and monensin, displayed potent inhibitory effects on cell proliferation at low concentrations of 10 ~ 100 nM (Fig. 6A). We subjected the cells to combined VEN/DAC and

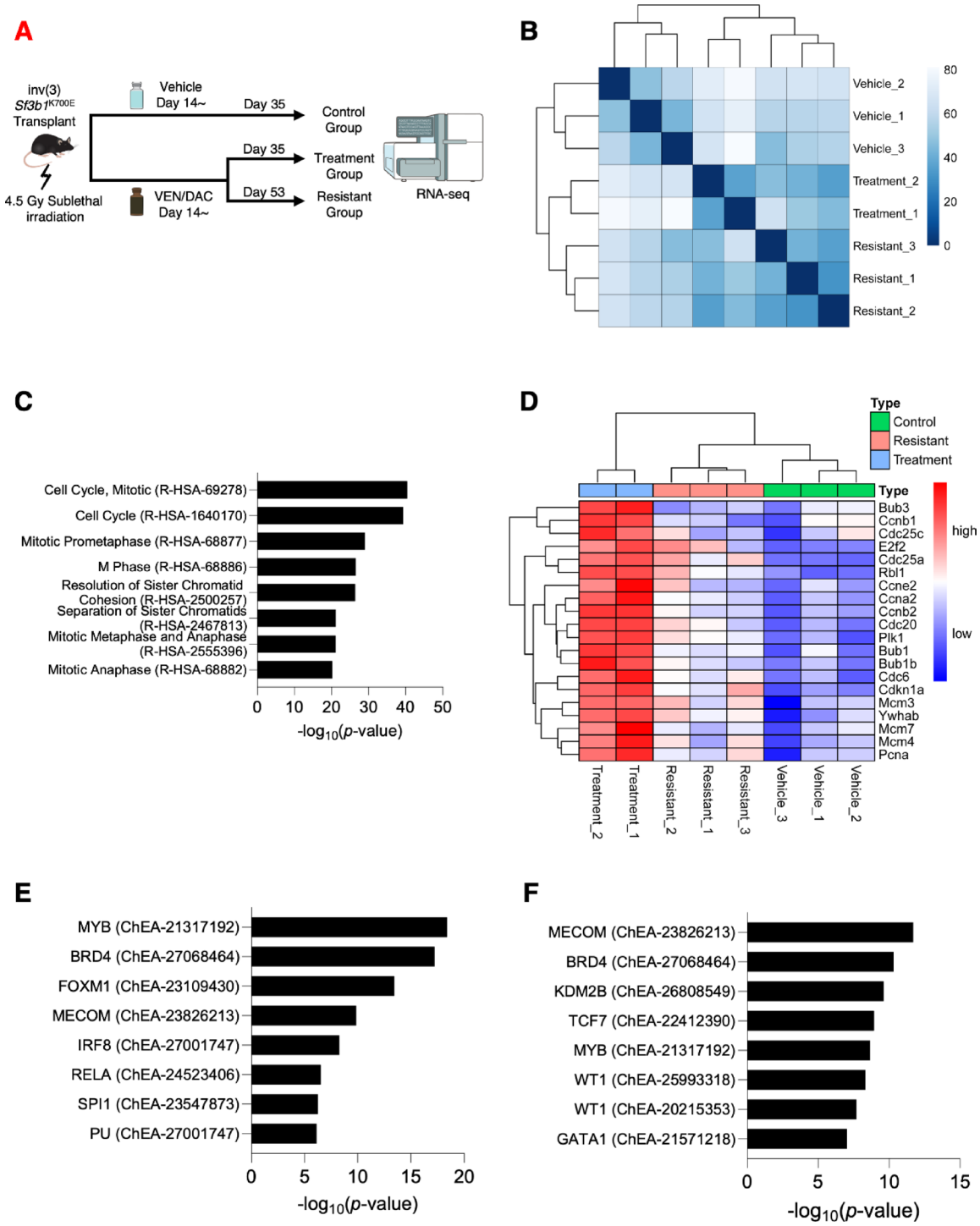

Fig. 4. Differential gene expression and transcriptional factor analysis in the treated and resistant groups. (**A**) Experimental schema of sample preparation used in RNA-seq analysis in VEN/DAC-treated inv(3) *Sf3b1*^{K700E} AML model. (**B**) Heatmap of the sample-to-sample distances and hierarchical clustering of 3 groups (Vehicle, VEN/DAC treatment, VEN/DAC resistance) by differential gene expression. (**C**) Reactome Pathway Analysis enrichment of genes upregulated in VEN/DAC treatment group compared with resistance mice, the *p*-values were calculated via Enrichr. (**D**) Heatmap and hierarchical clustering showing the expression of 20 cell cycle-associated genes in Vehicle, VEN/DAC treatment, and VEN/DAC resistance group. (**E**) ChIP Enrichment Analysis (ChEA) Transcription Factor Targets dataset analysis of genes upregulated in VEN/DAC treatment group compared to Vehicle group. The *p*-values were calculated via Enrichr; the x-axis represents -log10 of *p*-values. (**F**) ChEA Transcription Factor Targets dataset analysis of genes upregulated in VEN/DAC resistant group compared to Vehicle group, The *p*-values were calculated via Enrichr; the x-axis represents -log10 of *p*-values.

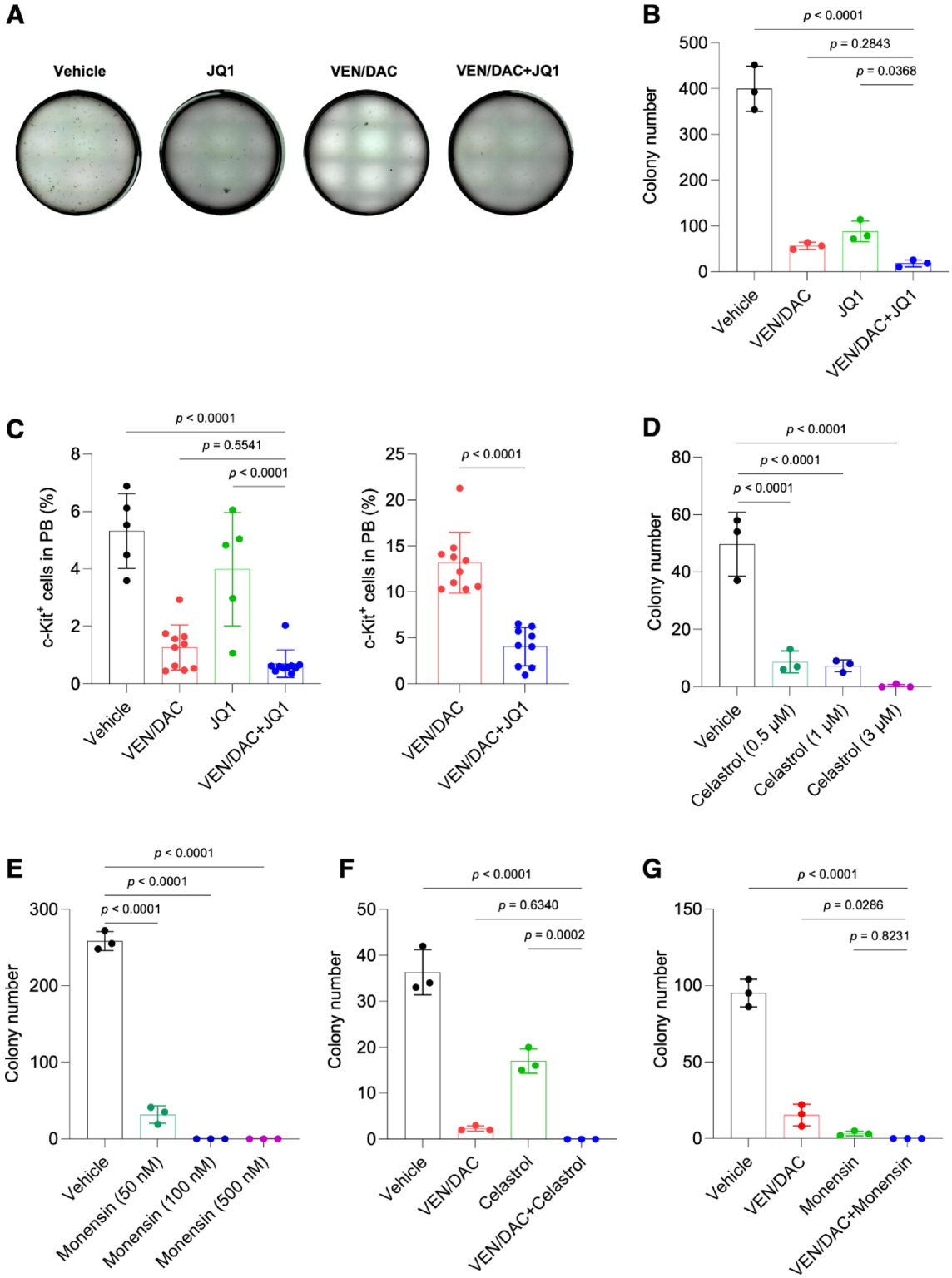

MYB inhibitors and analyzed their synergistic interactions using the highest single agent (HSA) or the Loewe models from SynergyFinder[35]. We observed that VEN/DAC and MYB inhibitor celastrol demonstrated a high level of synergy, with the maximal synergy score centered around 1 μM celastrol and 100 nM VEN/DAC (Fig. 6B, Supplementary Fig. 5A), consistent with the colony formation assay results from the mouse model (Fig. 5C, D). Another MYB inhibitor, monensin, exhibited an even more pronounced synergistic effect with VEN/DAC, featuring a lower threshold concentration and a broader synergy range (Fig. 6C, Supplementary Fig. 5B). Similarly, the BRD4 inhibitor JQ1 exhibited a robust synergistic effect with VEN/DAC at a concentration of 1 μM, reaching a high peak and highlighting its comparable therapeutic potential (Fig. 6D, Supplementary Fig. 5C). To validate monensin's effects on human cells, we investigate the YCU-AML1 cells' colony-forming capacity using an H4230 semi-solid medium. Colony counts on day 14 revealed a dose-dependent reduction in colony

◀**Fig. 5**. Treatment efficacy with BRD4/MYB inhibitors in inv(3) AML cells. (**A**) Representative images of M3434 colonies from inv(3) *Sf3b1*^{K700E} primary bone marrow cells with drug treatments (Vehicle, VEN/DAC, JQ1, and VEN/DAC + JQ1). The final concentration of all drugs in the semi-solid medium was 100 nM. (**B**) The number of colonies in methylcellulose M3434 is plotted in the right bar graph. $n = 3$ independent experiments; data represent mean ± s.e.m. The p-value relative to Vehicle by a two-sided t-test. (**C**) Frequency of c-Kit$^+$ cells in Vehicle group ($n = 5$ independent samples), VEN/DAC (day 21: $n = 10$ independent samples), JQ1 ($n = 5$ independent samples), VEN/DAC + JQ1 ($n = 10$ independent samples) at day 7 and day 42 post-drug treatment. Data represent mean ± s.e.m. The p-value was calculated by a two-sided t-test. (**D**) The number of colonies replaced in methylcellulose M3434 with Vehicle or celastrol (0.5 μM, 1 μM, or 3 μM), $n = 3$ independent experiments; data represent mean ± s.e.m. The p-value relative to Vehicle by a two-sided t-test. (**E**) The number of colonies replaced in methylcellulose M3434 with Vehicle or monensin (50 nM, 100 nM, or 500 nM), $n = 3$ independent experiments; data represent mean ± s.e.m. The p-value relative to Vehicle by a two-sided t-test. (**F**) The number of colonies cultured in methylcellulose M3434 with Vehicle or drugs at a final concentration of 100 nM (VEN/DAC, Celastrol, or VEN/DAC + Celastrol). $n = 3$ independent experiments; data represent mean ± s.e.m. The p-value relative to VEN/DAC + Celastrol by a two-sided t-test. (**G**) The number of colonies cultured in methylcellulose M3434 with 4 groups of different drug addiction components at a final concentration of 100 nM (Vehicle, VEN/DAC, Monensin, VEN/DAC + Monensin). $n = 3$ independent experiments; data represent mean ± s.e.m. The p-value relative to VEN/DAC + Monensin group by a two-sided t-test.

formation with increasing monensin concentration (Supplementary Fig. 5D). Finally, we evaluated the YCU-AML1 cell line cultured in H4230 medium to further validate the synergy between VEN/DAC and multiple MYB/BRD4 inhibitors. While VEN/DAC alone significantly suppressed colony growth, the addition of MYB or BRD4 inhibitors further enhanced this inhibition, demonstrating a strong synergistic effect (Fig. 6E-G). We also validated the synergistic effect of these BRD4 or MYB inhibitors in combination with VEN/DAC in another *EVI1*-rearranged and *SF3B1*-mutated cell line, MUTZ-3[11] (Supplementary Fig. 5E–G). In addition, Western blot analysis confirmed that the MYB inhibitors celastrol and monensin effectively suppressed the expression of c-MYB, c-MYB (phospho S11)[36,37], and its downstream target, c-MYC[38] (Fig. 6H, Supplementary Fig. 5H). These findings suggested that combining VEN/DAC and BRD4/MYB inhibitors is an effective treatment strategy for the poor prognostic inv(3) AML and overcomes the resistant mechanisms.

Discussion

AML with inv(3)/t(3;3) or elevated *EVI1* expression represents a particularly challenging therapeutic landscape. The aggressive nature of this subtype correlates with poor prognosis, as evidenced by the median overall survival of less than one year[39]. EVI1, a transcription factor that, when overexpressed, drives abnormal hematopoiesis and promotes stem-like properties in leukemic cells, becomes a pivotal player in therapeutic resistance[9]. The aberrant activation of *EVI1* through chromosomal rearrangements not only enhances self-renewal capabilities but also fosters chemotherapy resistance[10]. This highlights a paradox where the very mechanisms that confer a growth advantage to leukemic cells simultaneously render them less responsive to current therapies, such as venetoclax-containing regimens. Recent studies have underscored the heterogeneity observed within *EVI1*-high leukemias, varying degrees of *EVI1* expression, and frequent co-occurrence of mutations, such as those in *SF3B1*[11]. These mutations further complicate treatment strategies by contributing to pathological splicing changes, altered apoptotic signaling, and enhanced leukemic cell survival[11]. As such, this complexity necessitates a multifaceted approach to therapy, targeting not only the malignant cells but also the pathways that promote their survival.

The challenge of venetoclax resistance in AML, particularly in the context of *EVI1*-rearranged leukemias, is increasingly recognized as a significant barrier to effective treatment. Our study elucidates that inv(3)/t(3;3) AML cells possess intrinsic resistance to venetoclax, as indicated by reduced sensitivity in in vitro assays (Fig. 1A). This resistance is compounded by the frequent co-occurrence of mutations in splicing factors such as *SF3B1*, which exacerbat disease progression through pathological splicing and enhanced survival signaling[40]. The identification of transcriptional programs associated with venetoclax resistance offers potential avenues to enhance therapeutic efficacy. These findings underscore the importance of understanding transcriptional programs that underlie resistance to identify new therapeutic targets. Transcription factors such as MYB and BRD4 regulate key oncogenic and epigenetic processes that enable leukemic cells to survive therapeutic pressure. Recent literature suggests that targeting these pathways can sensitize resistant cells to venetoclax, highlighting the necessity for combination therapies that address the multifactorial nature of resistance[40,41]. By integrating inhibitors of BRD4 and MYB alongside conventional agents like venetoclax and hypomethylating agents, we may be able to disrupt the adaptive mechanisms employed by leukemia cells to evade therapy, thereby improving treatment outcomes.

The application of MYB and BRD4 inhibitors represents a promising strategy to enhance therapeutic efficacy in AML, particularly in *EVI1*-high subtypes. For example, Smeenk et al. demonstrated the requirement of MYB for oncogenic *EVI1* hyperactivation at the translocated enhancer caused by inv(3) or t(3;3)[42]. Our findings indicate that the combination of MYB inhibitors, such as celastrol and monensin, with venetoclax and decitabine enhances the cytotoxic effects on inv(3) AML cells, demonstrating significant synergy in colony formation assays (Fig. 5D and F). This is consistent with previous studies that highlight MYB as a critical transcription factor in the maintenance of leukemic stem cell properties and resistance to apoptosis[40]. Similarly, BRD4 has emerged as a crucial regulator of oncogenic transcriptional programs, and its inhibition has been shown to disrupt the

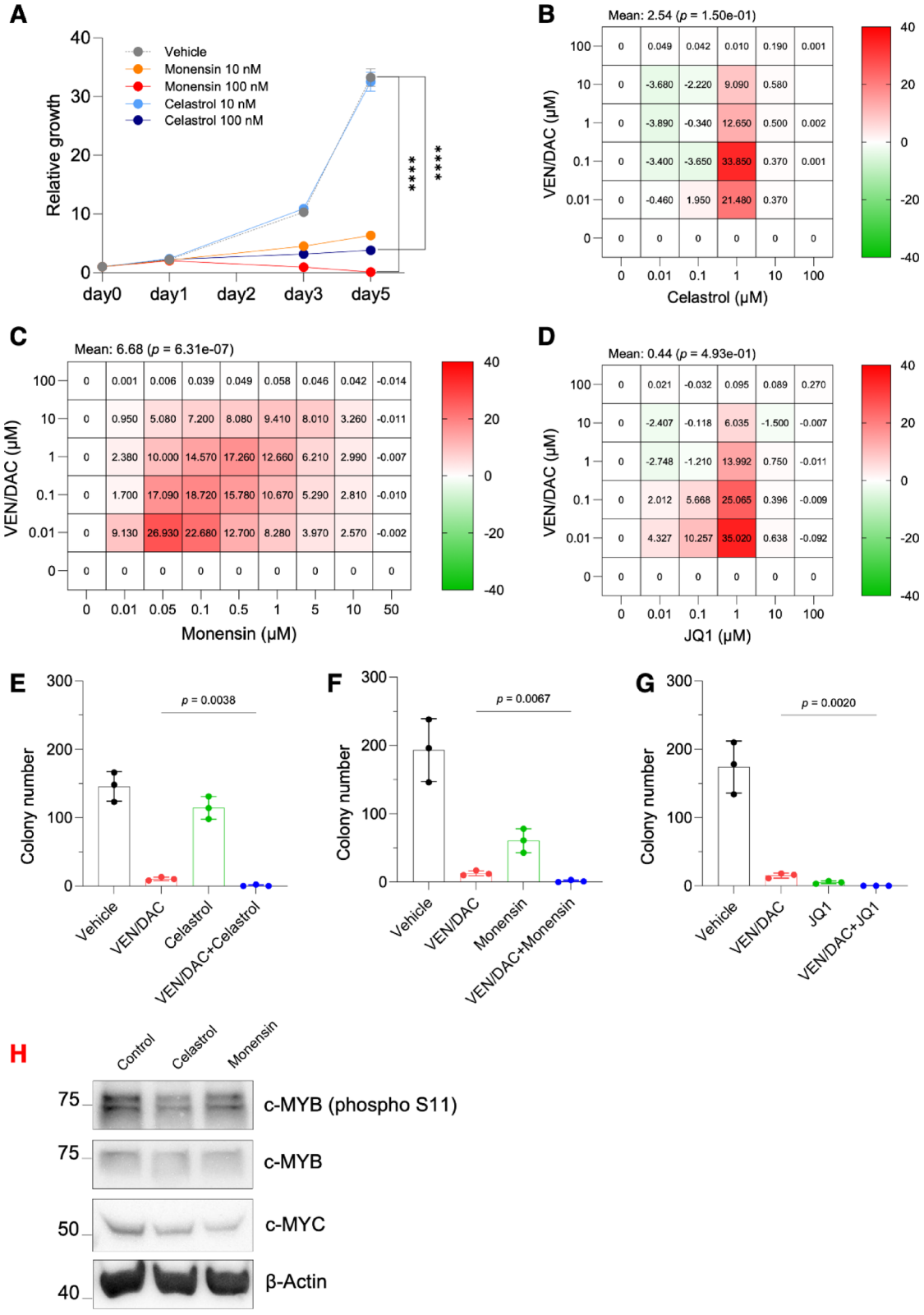

survival of AML cells, especially those with high *EVI1* expression[40,43,44]. The integration of these inhibitors into treatment regimens could potentially mitigate the resistance mechanisms that currently limit the effectiveness of venetoclax in *EVI1*-rearranged AML. However, while early results are promising, further investigations are warranted to elucidate the optimal dosing strategies and combinations that maximize therapeutic benefit while minimizing toxicity[40,41]. The persistence of resistant clones despite combination therapies highlights the necessity of identifying and targeting emergent vulnerabilities in resistant cells. Future studies should focus on the specific mechanisms through which BRD4, MYB, and MECOM drive resistance, as well as on the integration of these pathways with broader signaling networks. Additionally, addressing the pharmacokinetics

◀**Fig. 6**. Synergistic effects in human patient-derived inv(3) leukemic cells. (**A**) Relative cell viability of YCU-AML1 with MYB inhibitor treatment was measured using a luminescent cell viability assay; the y-axis is the intensity ratio based on Day 0. (**B**) Heatmap of the synergistic score for the combination treatment of VEN/DAC and celastrol at day 3. SynergyFinder analyzed the data under the highest single agent (HSA) complete models for combination analysis. Red colors indicate synergistic points, green points indicate antagonistic points. (**C**) Heatmap of the synergistic score for the combination treatment of VEN/DAC and monensin at day 3. SynergyFinder analyzed the data under the highest single agent (HSA) complete models for combination analysis. Red colors indicate synergistic points, green points indicate antagonistic points. (**D**) Heatmap of the synergistic score for the combination treatment of VEN/DAC and JQ1 at day 3. SynergyFinder analyzed the data under the highest single agent (HSA) complete models for combination analysis. Red colors indicate synergistic points, green points indicate antagonistic points. (**E**) In vitro colony-forming assay cultured with human GM-CSF (10 ng/mL) and either Vehicle or drugs at a final concentration of 100 nM (VEN/DAC, Celastrol, or VEN/DAC + Celastrol). $n = 3$ independent experiments; data represent mean ± s.e.m. The p-value relative to VEN/DAC group by a two-sided t-test. (**F**) In vitro colony-forming assay cultured with human GM-CSF (10 ng/mL) and either Vehicle or drugs at a final concentration of 100 nM (VEN/DAC, Monensin, or VEN/DAC + Monensin). $n = 3$ independent experiments; data represent mean ± s.e.m. The p-value relative to VEN/DAC group by a two-sided t-test. (**G**) In vitro colony-forming assay cultured with human GM-CSF (10 ng/mL) and either Vehicle or drugs at a final concentration of 100 nM (VEN/DAC, JQ1, or VEN/DAC + JQ1). $n = 3$ independent experiments; data represent mean ± s.e.m. The p-value relative to VEN/DAC group by a two-sided t-test. (**H**) Immunoblot analysis of phosphorylated c-MYB, total c-MYB, c-MYC, and β-Actin in protein extracts from MUTZ-3 cells cultured with DMSO (Control), Celastrol 1 μM, or Monensin 1 μM for 24 h.

and pharmacodynamics of these inhibitors will be crucial for improving their in vivo efficacy. Overall, our study contributes to the growing body of evidence advocating for a targeted approach in treating *EVI1*-high AML, emphasizing the importance of understanding molecular underpinnings in the development of effective therapies.

In summary, addressing the challenges posed by inv(3)/ t(3;3) AML and *EVI1*-high leukemias requires a multifaceted approach that includes overcoming venetoclax resistance and leveraging novel therapeutic strategies involving MYB and BRD4 inhibition. Our findings emphasize the importance of understanding molecular mechanisms of resistance and integrating this knowledge into innovative treatment strategies. By continuing to explore these avenues, we may pave the way for more effective and personalized treatment options for patients suffering from this aggressive form of leukemia.

Methods

Clinical data analysis

Venetoclax sensitivity was calculated based on data from AML patients[45], and compared between *EVI1*-rearranged patients (n = 4) versus others (non-*EVI1*-rearranged) (n = 55), and between low (n = 67) versus high (n = 13) *MECOM* mRNA expression groups. The p-values were calculated using a two-sided t-test. The mutational frequencies of the most frequently mutated genes in inv(3)/t(3;3) patients[18–20] (*SF3B1*, *NRAS*, *PTPN11*, *KRAS*, *TP53*, *DNMT3A*, *GATA2*, *ASXL1*, *NF1*, *FLT3*, *RUNX1*, and *KIT*) were calculated based on data from inv(3)/t(3;3) AML patients (n = 109), the Beat AML cohort (n = 622), and the TCGA AML cohort (n = 200). The p-values were calculated using Fisher's exact test applied to 2 × 2 contingency tables comparing *EVI1*-rearrangement negative and *EVI1*-rearrangement positive samples based on mutated versus unmutated gene status.

Animals and ethical approval

inv(3)(3q21q26) mouse strain (RBRC09508) was provided by RIKEN BRC through the National BioResource Project of the MEXT/AMED, Japan. NOD/SCID-IL2Rgnull (NSG) mice were purchased from Charles River Laboratories Japan (Yokohama, Japan). All animals were housed at the Foundation for Biomedical Research and Innovation (FBRI, Japan) using a 12-hour light/12-hour dark cycle at an ambient temperature of 21.5 °C ± 1 °C and 30% to 70% humidity. All animal procedures were followed by the Guidelines for the Care and Use of Laboratory Animals and approved by the Institutional Animal Care and Use Committees at FBRI. All mouse experiments were performed according to a protocol approved by the FBRI Institutional Animal Care and Use Committee. All animal experiments were followed by the ARRIVE guidelines. All experimental methods were performed in accordance with a protocol approved by the formal ethics committee at FBRI, under approval No. 22-08.

Cell lines

The YCU-AML1 cell line was previously established from a patient-derived xenograft (PDX) model of a high-risk MDS/AML patient with the t(3;3)(q21;q26.2) mutation, as reported by Kunimoto et al.[34]. The detailed methodology is outlined in prior literature[34].

Bone marrow (BM) transplantation

Freshly dissected femora and tibiae were isolated from inv(3) *Sf3b1*$^{K700E/WT}$ mice. BM was flushed with a 3 mL insulin syringe into PBS supplemented with 3% fetal bovine serum (FBS). The BM was spun at 500 g by centrifugation, and RBCs were lysed in ammonium chloride-potassium bicarbonate lysis buffer for 5 min. After centrifugation, cells were resuspended in PBS supplemented with 2% FBS, passed through a cell strainer, and

counted. Washed BM cells were transplanted via tail vein injection into sublethally irradiated (4.5 Gy) CD45.1$^+$ recipient mice. YCU-AML1 cells were transplanted via tail vein injection into sublethally irradiated (2.0 Gy) NSG (NOD.Cg-*Prkdc*^{scid}*Il2rg*^{tm1Wjl}/SzJ) mice.

In vitro colony formation assays

Whole BM cells from inv(3) *Sf3b1*$^{K700E/WT}$ primary leukemic mice or VEN/DAC-resistant clone mice were seeded at a density of 10,000 cells/replicate in cytokine-supplemented methylcellulose semi-solid medium (Methocult M3434, STEMCELL Technologies). Colonies were cultured at 37 °C and 5% CO_2 and counted on day 7. YCU-AML1 cells were seeded at a density of 2.0×10^5 cells/well by triplicate into cytokine-free methylcellulose medium (Methocult H4230, STEMCELL Technologies) with GM-CSF 10 ng/mL. Plates were placed into an incubator at 37 °C and 5% CO_2, and colonies were counted on day 14.

Antibodies

All FACS antibodies were purchased from eBioscience and BioLegend. BM mononuclear cells were stained with a lineage cocktail consisting of antibodies targeting CD3, B220, Gr-1, CD11b, and Ter-119. Cells were also stained with antibodies against c-Kit, anti-mouse CD45, and anti-human CD45. Cell populations were analyzed using FACS Lyric (BD Biosciences). We used the following antibodies: B220-PECy7 (clone: RA3-6B2; BD Pharmingen; catalog #:10322; dilution: 1:300); CD3-APCCy7 (145-2c11; BioLegend; 100330; 1:300); Gr-1-APC (RB6-8C5; BD Pharmingen; 553129; 1:300); CD11b-PerCPCy5.5 (M1/70; Biolegend; 101228; 1:300); c-Kit-FITC (2B8; eBioscience; 553354; 1:300); anti-mouse CD45-PerCPCy5.5 (2B8; Biolegend; 105824; 1:1000) and anti-human CD45-BV510 (HI30; Biolegend; 304036; 1:100). The following antibodies were used for Western Blot analysis: c-Myb (phospho S11) (ab45150; Abcam; 1:1000), c-Myb (#59995; Cell Signaling; 1:1000), c-Myc (#5605; Cell Signaling; 1:1000), and β-Actin (A5441; Sigma-Aldrich; 1:5000).

Peripheral blood analysis

Blood was collected by bleeding from the mouse tail using a heparinized microhematocrit capillary tube (Thermo Fisher Scientific). Peripheral blood counts were automated using a HemaVet 950 (Drew Scientific).

Histological analysis with Wright-Giemsa staining

Bone marrow cells were collected and prepared for morphological analysis using cytospin centrifugation. Briefly, 1×10^5 cells were centrifuged onto glass slides at 650 rpm for 5 minutes using a cytocentrifuge. Slides were air-dried at room temperature and stained by using Hemacolor Rapid staining of blood smear (#1.11957.2500, Sigma-Aldrich), according to the standard manufacturer's protocols.

Cell culture

YCU-AML1 cells were cultured in OP-9 cell culture supernatant (Minimum Essential Medium α (α-MEM) containing 20% fetal bovine serum (FBS)) supplemented with GM-CSF (10 ng/mL). MUTZ-3 cells (purchased from DSMZ) were cultured in α-MEM containing 20% FBS and 20% supernatant from the 5637 cell line.

In vitro cell viability assays

YCU-AML1 cells were seeded in white flat-well 96-well plates (Costar) at a density of 10,000 cells per well with the supernatant of OP-9 cell culture medium (Minimum Essential Medium α/20% FBS). ATP luminescence readings were taken 24 h, 72 h, and 128 h after seeding, using Cell Titer Glo (Promega) according to the manufacturer's instructions.

Chemicals

Venetoclax (A-1195425.0) was obtained from Abbvie and dissolved in 60% Phosal 50PG/30% PEG400/10% Ethanol. Other drugs used in the experiments: JQ1 (MCE, HY-1303), ABBV-744 (Selleck, S8723), celastrol (Sigma-Aldrich, C0869), and monensin sodium salt (purity 90–95% TLC) (Sigma-Aldrich, M5273) were dissolved in DMSO.

In vivo drug treatment

Recipient mice transplanted with inv(3) *Sf3b1*$^{K700E/WT}$ leukemia cells were administered venetoclax (100 mg/kg, once daily, by oral gavage) and decitabine (0.25 mg/kg, every 48 h via intraperitoneal injection) for three weeks, beginning at day 14 post-transplantation.

mRNA isolation and bulk RNA sequencing

For MACS-sorted c-Kit$^+$ cells using CD117 MicroBeads (MACS, Miltenyi Biotec), RNA was extracted using RNeasy columns (Qiagen) according to the manufacturer's instructions, followed by poly(A)-select treatment of the RNA and preparation of Illumina stranded libraries using the TruSeq Stranded mRNA Library Preparation Kit. Libraries were sequenced on an Illumina NovaSeq 6000 at a depth of ~ 30 M 2 × 151 bp reads per sample. For differential expression analysis, FASTQ sequenced reads were filtered by Fastp and mapped to mm10 using hisat2[46,47]. Gene counts were calculated with featureCounts[48], normalized and differentially expressed genes with adjusted *p*-values of less than 0.1 were identified using DESeq2[49] and weighted using an independent hypothesis (Supplementary Table 1). Variance-stabilized transformed data calculated by the DESeq2-vsd function were used for hierarchical clustering and principal component analysis. Gene ontology was performed using Enrichr[50–52].

Two-drug synergistic analysis

YCU-AML1 and MUTZ-3 were seeded into 96-well plates at a density of 10,000 cells per well. Drug combinations of VEN/DAC with JQ1, celastrol, or monensin were added to the growth medium at varying concentrations. Cells were incubated with the drugs for 72 h at 37 °C and 5% CO_2. ATP luminescence readings were measured using CellTiter-Glo (Promega) according to the manufacturer's instructions. Synergistic scores based on the cell viability assay were calculated using the SynergyFinder web tool[35].

Statistical analysis

Statistical analyses were performed using R (version 4.3.3), GraphPad Prism (version 10), DESeq2 (version 1.49.3), Enrichr (version 3.4), and SynergyFinder (version 3.16.0). Statistical significance was calculated using two-tailed unpaired t-test, log-rank test, two-sided Wilcoxon rank-sum test, Fisher's exact test, one-way ANOVA, binomial distribution in Enrichr, and bootstrapping in SynergyFinder, as indicated in the figure legends. The number of mice in each group and the number of replicates for each experiment are shown in the figure legends. All error bars represent mean ± s.e.m.

Data availability

Sequencing data generated in this study have been deposited in the Gene Expression Omnibus (GEO) under accession number GSE292744 (RNA-seq).

Received: 31 March 2025; Accepted: 18 September 2025
Published online: 23 October 2025

References

1. Sun, J. et al. De Novo acute myeloid leukemia with inv(3)(q21q26.2) or t(3;3)(q21;q26.2): A clinicopathologic and cytogenetic study of an entity recently added to the WHO classification. *Mod. Pathol.* **24**, 384–389. https://doi.org/10.1038/modpathol.2010.210 (2011).
2. Lugthart, S. et al. Clinical, molecular, and prognostic significance of WHO type inv(3)(q21q26.2)/t(3;3)(q21;q26.2) and various other 3q abnormalities in acute myeloid leukemia. *J. Clin. Oncol.* **28**, 3890–3898. https://doi.org/10.1200/JCO.2010.29.2771 (2010).
3. Cui, W., Sun, J., Cotta, C. V., Medeiros, L. J. & Lin, P. Myelodysplastic syndrome with inv(3)(q21q26.2) or t(3;3)(q21;q26.2) has a high risk for progression to acute myeloid leukemia. *Am. J. Clin. Pathol.* **136**, 282–288. https://doi.org/10.1309/AJCP48AJDCKTHUXC (2011).
4. Rogers, H. J. et al. Complex or monosomal karyotype and not blast percentage is associated with poor survival in acute myeloid leukemia and myelodysplastic syndrome patients with inv(3)(q21q26.2)/t(3;3)(q21;q26.2): A bone marrow pathology group study. *Haematologica* **99**, 821–829. https://doi.org/10.3324/haematol.2013.096420 (2014).
5. Groschel, S. et al. High EVI1 expression predicts outcome in younger adult patients with acute myeloid leukemia and is associated with distinct cytogenetic abnormalities. *J. Clin. Oncol.* **28**, 2101–2107. https://doi.org/10.1200/JCO.2009.26.0646 (2010).
6. Summerer, I. et al. Prognosis of MECOM (EVI1)-rearranged MDS and AML patients rather depends on accompanying molecular mutations than on blast count. *Leuk. Lymphoma.* **61**, 1756–1759. https://doi.org/10.1080/10428194.2020.1737689 (2020).
7. Yamazaki, H. et al. A remote GATA2 hematopoietic enhancer drives leukemogenesis in inv(3)(q21;q26) by activating EVI1 expression. *Cancer Cell.* **25**, 415–427. https://doi.org/10.1016/j.ccr.2014.02.008 (2014).
8. Groschel, S. et al. A single oncogenic enhancer rearrangement causes concomitant EVI1 and GATA2 deregulation in leukemia. *Cell* **157**, 369–381. https://doi.org/10.1016/j.cell.2014.02.019 (2014).
9. Perkins, A. S., Fishel, R., Jenkins, N. A. & Copeland, N. G. Evi-1, a murine zinc finger proto-oncogene, encodes a sequence-specific DNA-binding protein. *Mol. Cell. Biol.* **11**, 2665–2674. https://doi.org/10.1128/mcb.11.5.2665-2674.1991 (1991).
10. Birdwell, C. et al. EVI1 dysregulation: Impact on biology and therapy of myeloid malignancies. *Blood Cancer J.* **11**, 64. https://doi.org/10.1038/s41408-021-00457-9 (2021).
11. Tanaka, A. et al. Aberrant EVI1 splicing contributes to EVI1-rearranged leukemia. *Blood* **140**, 875–888. https://doi.org/10.1182/blood.2021015325 (2022).
12. DiNardo, C. D. et al. Venetoclax combined with decitabine or Azacitidine in treatment-naive, elderly patients with acute myeloid leukemia. *Blood* **133**, 7–17. https://doi.org/10.1182/blood-2018-08-868752 (2019).
13. Certo, M. et al. Mitochondria primed by death signals determine cellular addiction to antiapoptotic BCL-2 family members. *Cancer Cell.* **9**, 351–365. https://doi.org/10.1016/j.ccr.2006.03.027 (2006).
14. Souers, A. J. et al. ABT-199, a potent and selective BCL-2 inhibitor, achieves antitumor activity while sparing platelets. *Nat. Med.* **19**, 202–208. https://doi.org/10.1038/nm.3048 (2013).
15. DiNardo, C. D. et al. Azacitidine and venetoclax in previously untreated acute myeloid leukemia. *N Engl. J. Med.* **383**, 617–629. https://doi.org/10.1056/NEJMoa2012971 (2020).
16. Russo, D. et al. Venetoclax plus decitabine as a Bridge to allogeneic Haematopoietic stem-cell transplantation in older patients with acute myeloid leukaemia (VEN-DEC GITMO): Final report of a multicentre, single-arm, phase 2 trial. *Lancet Haematol.* **11**, e830–e838. https://doi.org/10.1016/S2352-3026(24)00241-2 (2024).
17. Russell, M. et al. Expression of EVI1 in myelodysplastic syndromes and other hematologic malignancies without 3q26 translocations. *Blood* **84**, 1243–1248 (1994).
18. Groschel, S. et al. Mutational spectrum of myeloid malignancies with inv(3)/t(3;3) reveals a predominant involvement of RAS/RTK signaling pathways. *Blood* **125**, 133–139. https://doi.org/10.1182/blood-2014-07-591461 (2015).
19. Lavallee, V. P. et al. EVI1-rearranged acute myeloid leukemias are characterized by distinct molecular alterations. *Blood* **125**, 140–143. https://doi.org/10.1182/blood-2014-07-591529 (2015).
20. Tyner, J. W. et al. Functional genomic landscape of acute myeloid leukaemia. *Nature* **562**, 526–531. https://doi.org/10.1038/s41586-018-0623-z (2018).
21. Bottomly, D. et al. Integrative analysis of drug response and clinical outcome in acute myeloid leukemia. *Cancer Cell* **40**, 850–864 e859, (2022). https://doi.org/10.1016/j.ccell.2022.07.002
22. Obeng, E. A. et al. Physiologic expression of Sf3b1(K700E) causes impaired erythropoiesis, aberrant splicing, and sensitivity to therapeutic spliceosome modulation. *Cancer Cell.* **30**, 404–417. https://doi.org/10.1016/j.ccell.2016.08.006 (2016).
23. Cross, M., Mangelsdorf, I., Wedel, A. & Renkawitz, R. Mouse lysozyme M gene: Isolation, characterization, and expression studies. *Proc. Natl. Acad. Sci. U S A.* **85**, 6232–6236. https://doi.org/10.1073/pnas.85.17.6232 (1988).
24. Kharitonenkov, A. et al. A family of proteins that inhibit signalling through tyrosine kinase receptors. *Nature* **386**, 181–186. https://doi.org/10.1038/386181a0 (1997).
25. Zhang, D. E. et al. Absence of granulocyte colony-stimulating factor signaling and neutrophil development in CCAAT enhancer binding protein alpha-deficient mice. *Proc. Natl. Acad. Sci. U S A.* **94**, 569–574. https://doi.org/10.1073/pnas.94.2.569 (1997).

26. Lekstrom-Himes, J. A., Dorman, S. E., Kopar, P., Holland, S. M. & Gallin, J. I. Neutrophil-specific granule deficiency results from a novel mutation with loss of function of the transcription factor CCAAT/enhancer binding protein epsilon. *J. Exp. Med.* **189**, 1847–1852. https://doi.org/10.1084/jem.189.11.1847 (1999).
27. Buaas, F. W. et al. Plzf is required in adult male germ cells for stem cell self-renewal. *Nat. Genet.* **36**, 647–652. https://doi.org/10.1038/ng1366 (2004).
28. Lee, J. S. et al. The insulin and IGF signaling pathway sustains breast cancer stem cells by IRS2/PI3K-mediated regulation of MYC. *Cell. Rep.* **41**, 111759. https://doi.org/10.1016/j.celrep.2022.111759 (2022).
29. Shah, M. A. & Schwartz, G. K. Cell cycle-mediated drug resistance: An emerging concept in cancer therapy. *Clin. Cancer Res.* **7**, 2168–2181 (2001).
30. Filippakopoulos, P. et al. Selective Inhibition of BET bromodomains. *Nature* **468**, 1067–1073. https://doi.org/10.1038/nature09504 (2010).
31. Faivre, E. J. et al. Selective Inhibition of the BD2 bromodomain of BET proteins in prostate cancer. *Nature* **578**, 306–310. https://doi.org/10.1038/s41586-020-1930-8 (2020).
32. Uttarkar, S. et al. Targeting acute myeloid leukemia with a small molecule inhibitor of the Myb/p300 interaction. *Blood* **127**, 1173–1182. https://doi.org/10.1182/blood-2015-09-668632 (2016).
33. Yusenko, M. V. et al. Monensin, a novel potent MYB inhibitor, suppresses proliferation of acute myeloid leukemia and adenoid cystic carcinoma cells. *Cancer Lett.* **479**, 61–70. https://doi.org/10.1016/j.canlet.2020.01.039 (2020).
34. Kunimoto, H. et al. Establishment of a high-risk MDS/AML cell line YCU-AML1 and its xenograft model harboring t(3;3) and monosomy 7. *Hemasphere* **4**, e469. https://doi.org/10.1097/HS9.0000000000000469 (2020).
35. Zheng, S. et al. SynergyFinder plus: Toward better interpretation and annotation of drug combination screening datasets. *Genomics Proteom. Bioinf.* **20**, 587–596. https://doi.org/10.1016/j.gpb.2022.01.004 (2022).
36. Ramsay, R. G. et al. Regulation of c-Myb through protein phosphorylation and leucine zipper interactions. *Oncogene* **11**, 2113–2120 (1995).
37. Cures, A., House, C., Kanei-Ishii, C., Kemp, B. & Ramsay, R. G. Constitutive c-Myb amino-terminal phosphorylation and DNA binding activity uncoupled during entry and passage through the cell cycle. *Oncogene* **20**, 1784–1792. https://doi.org/10.1038/sj.onc.1204345 (2001).
38. Nakagoshi, H., Kanei-Ishii, C., Sawazaki, T., Mizuguchi, G. & Ishii, S. Transcriptional activation of the c-myc gene by the c-myb and B-myb gene products. *Oncogene* **7**, 1233–1240 (1992).
39. Sitges, M. et al. Acute myeloid leukemia with inv(3)(q21.3q26.2)/t(3;3)(q21.3;q26.2): Study of 61 patients treated with intensive protocols. *Eur. J. Haematol.* **105**, 138–147. https://doi.org/10.1111/ejh.13417 (2020).
40. Garciaz, S., Hospital, M. A., Collette, Y. & Vey, N. Venetoclax resistance in acute myeloid leukemia. *Cancers (Basel)*. https://doi.org/10.3390/cancers16061091 (2024).
41. Klempnauer, K. H. Transcription factor MYB as therapeutic target: Current developments. *Int. J. Mol. Sci.* https://doi.org/10.3390/ijms25063231 (2024).
42. Smeenk, L. et al. Selective requirement of MYB for oncogenic hyperactivation of a translocated enhancer in leukemia. *Cancer Discov.* **11**, 2868–2883. https://doi.org/10.1158/2159-8290.CD-20-1793 (2021).
43. Birdwell, C. E. et al. Preclinical efficacy of targeting epigenetic mechanisms in AML with 3q26 lesions and EVI1 overexpression. *Leukemia* **38**, 545–556. https://doi.org/10.1038/s41375-023-02108-3 (2024).
44. Nakamura, M. et al. Modelling and drug targeting of a myeloid neoplasm with atypical 3q26/MECOM rearrangement using patient-specific iPSCs. *Br. J. Haematol.* **205**, 1430–1443. https://doi.org/10.1111/bjh.19720 (2024).
45. Hashimoto, M. et al. Combined Inhibition of XIAP and BCL2 drives maximal therapeutic efficacy in genetically diverse aggressive acute myeloid leukemia. *Nat. Cancer.* **2**, 340–356. https://doi.org/10.1038/s43018-021-00177-w (2021).
46. Kim, D., Paggi, J. M., Park, C., Bennett, C. & Salzberg, S. L. Graph-based genome alignment and genotyping with HISAT2 and HISAT-genotype. *Nat. Biotechnol.* **37**, 907–915. https://doi.org/10.1038/s41587-019-0201-4 (2019).
47. Chen, S. Ultrafast one-pass FASTQ data preprocessing, quality control, and deduplication using Fastp. *Imeta* **2**, e107. https://doi.org/10.1002/imt2.107 (2023).
48. Liao, Y., Smyth, G. K. & Shi, W. FeatureCounts: An efficient general purpose program for assigning sequence reads to genomic features. *Bioinformatics* **30**, 923–930. https://doi.org/10.1093/bioinformatics/btt656 (2014).
49. Love, M. I., Huber, W. & Anders, S. Moderated Estimation of fold change and dispersion for RNA-seq data with DESeq2. *Genome Biol.* **15**, 550. https://doi.org/10.1186/s13059-014-0550-8 (2014).
50. Chen, E. Y. et al. Enrichr: Interactive and collaborative HTML5 gene list enrichment analysis tool. *BMC Bioinform.* **14**, 128. https://doi.org/10.1186/1471-2105-14-128 (2013).
51. Kuleshov, M. V. et al. Enrichr: A comprehensive gene set enrichment analysis web server 2016 update. *Nucleic Acids Res.* **44**, W90–97. https://doi.org/10.1093/nar/gkw377 (2016).
52. Xie, Z. et al. Gene set knowledge discovery with enrichr. *Curr. Protoc.* **1**, e90. https://doi.org/10.1002/cpz1.90 (2021).

Acknowledgements

The work received grant support and venetoclax from AbbVie, supported by JSPS KAKENHI (JP23K07824 to K.N., JP24H00866 to D.I., JP20H00537 to D.I., JP23H00430 to D.I., and JP24K21298 to D.I.), JST CREST (JPMJCR23B7 to D.I.), AMED (JP23ama221126 to D.I. and JP24ama221135 to K.N.), Japanese Society of Hematology (to D.I.), Ono Pharmaceutical Foundation for Oncology (to D.I.), The Mitsubishi Foundation (to D.I.), Kobayashi Foundation for Cancer Research (to D.I.), Takeda Science Foundation (to K.N. and D.I.), Chugai Foundation for Innovative Drug Discovery Science (to D.I.), Foundation for Promotion of Cancer Research (to D.I.), Princess Takamatsu Cancer Research Fund (to K.N.). The super-computing resource was provided by Human Genome Center (the University of Tokyo). Sequencer and Drug Illustration from NIAID NIH BIOART Source (bioart.niaid.nih.gov/bioart/386, bioart.niaid.nih.gov/bioart/536).

Author contributions

W.Z., K.N., F.I., A.T.-K., and D.I. designed the study; W.Z., Y.K., A.T., H.Y., T.Y., H.I., Y.Z., Y.A., W.S., M.X., and C.H. performed animal experiments. H.K. and H.M. established the YCU-AML1 cell lines. W.Z., F.I., and D.I. performed computational analyses of RNA-seq data; W.Z., K.N., and D.I. wrote the manuscript with approval from all co-authors.

Declarations

Competing interests

D.I. has received prior research funding and venetoclax compounds from Abbvie. No other potential conflict

of interest relevant to this article was reported. There are no competing interests of the other authors.

Additional information

Supplementary Information The online version contains supplementary material available at https://doi.org/10.1038/s41598-025-21034-1.

Correspondence and requests for materials should be addressed to K.N. or D.I.

Reprints and permissions information is available at www.nature.com/reprints.

Publisher's note Springer Nature remains neutral with regard to jurisdictional claims in published maps and institutional affiliations.